Nicotinamide Metabolism Modulates the Proliferation/Differentiation Balance and Senescence of Human Primary Keratinocytes

JID Open

Chye Ling Tan[1,4], Toby Chin[1,4], Christina Yan Ru Tan[1], Holly A. Rovito[2], Ling Shih Quek[1], John E. Oblong[2] and Sophie Bellanger[1,3]

Nicotinamide (NAM) is the main precursor of nicotinamide adenine dinucleotide (NAD^+), a coenzyme essential for DNA repair, glycolysis, and oxidative phosphorylation. NAM has anti-aging activity on human skin, but the underlying mechanisms of action are unclear. Using 3-dimensional organotypic skin models, we show that NAM inhibits differentiation of the upper epidermal layers and maintains proliferation in the basal layer. In 2-dimensional culture, NAM reduces the expression of early and late epidermal differentiation markers and increases the proliferative capacity of human primary keratinocytes. This effect is characterized by elevated clonogenicity and an increased proportion of human primary keratinocyte stem cell (holoclones) compared to controls. By contrast, preventing the conversion of NAM to NAD^+ using FK866 leads to premature human primary keratinocyte differentiation and senescence, together with a dramatic drop in glycolysis and cellular adenosine triphosphate levels while oxidative phosphorylation is moderately affected. All these effects are rescued by addition of NAM, known to compete with FK866, which suggests that conversion to NAD^+ is part of the mechanistic response. These data provide insights into the control of differentiation, proliferation, and senescence by NAM and NAD^+ in skin. They may lead to new therapeutic advances for skin conditions characterized by dysregulated epidermal homeostasis and premature skin aging, such as photoaging.

Journal of Investigative Dermatology (2019) **139,** 1638–1647; doi:10.1016/j.jid.2019.02.005

INTRODUCTION

Nicotinamide (NAM), also known as niacinamide or vitamin B-3, is a nicotinamide adenine dinucleotide (NAD^+) precursor that is rapidly incorporated into the NAD(H)/NADP(H) pool. NAM has beneficial effects on skin appearance, such as reducing melasma (Navarrete-Solis et al., 2011), sallowness, hyperpigmentation, and wrinkles (Bissett et al., 2004, 2005). It has thus been classified as an anti-aging molecule. However, the uses of NAM are not limited to the cosmetics field. Vitamin B-3 deficiency is associated with a number of skin lesions, including pellagra-associated dermatitis, acne, dermatoses, and actinic keratosis, and NAM is efficient at improving bullous pemphigoid (Fivenson et al., 1994) and psoriasis (Levine et al., 2010; Siadat et al., 2013). Furthermore, topical and oral administration of NAM can reduce onset of UV-induced immunosuppression, a critical mechanism involved in cancer induction (Damian et al., 2008; Gensler, 1997; Yiasemides et al., 2009), and prevent non-melanoma skin cancers (Chen et al., 2015; Kim et al., 2015). These findings highlight NAM as a promising molecule with multiple domains of application.

Although the positive effects of NAM on skin aging are clear, little is known about the underlying molecular pathways. NAM is converted to NAD^+ in the cytoplasm and nucleus by two successive reactions involving the enzymes NAMPT and NMNAT (Garten et al., 2015). NAD^+ levels decrease with age in skin and in many other tissues (Camacho-Pereira et al., 2016; Massudi et al., 2012; Yoshino et al., 2011), and data have started to identify the notable role of NAD^+ in longevity and human health (Chini et al., 2017; Imai and Guarente, 2016). NAM has thus been proposed to limit aging primarily by replenishing the NAD^+ pool, but how newly synthesized NAD^+ prevents aging is unclear.

Ablating NAMPT reduces the pool and proliferation of adult neural stem cells (Stein and Imai, 2014) and, interestingly, a link between stem cell loss (either due to a reduction in stem cell number or in stem cell function) and aging has been shown in different organisms, including some mammal adult tissues like brain, intestine, and muscles (Jones and Rando, 2011; Keyes and Fuchs, 2018). Regarding skin, the number of hair follicle stem cells has been shown to be stable over time (Giangreco et al., 2008). However, more recently, depletion of hair follicle stem cells in areas of severe hair loss has been published to occur in aged mice (Matsumura et al.,

[1]*Cell Cycle Control in Skin Epidermis, Skin Research Institute of Singapore, A*STAR, Singapore;* [2]*Beauty Technology Division, The Procter & Gamble Company, Cincinnati, Ohio, USA; and* [3]*School of Biological Sciences and Lee Kong Chian School of Medicine, Nanyang Technological University, Singapore*

[4]*These authors contributed equally to this work.*

*Correspondence: Sophie Bellanger, Cell Cycle Control in Skin Epidermis, Skin Research Institute of Singapore, A*STAR, 8A Biomedical Grove, Singapore 138648. E-mail: sophie_bellanger@sris.a-star.edu.sg*

Abbreviations: ATP, adenosine triphosphate; HPK, human primary keratinocyte; NAD, nicotinamide adenine dinucleotide; NAM, nicotinamide; OXPHOS, oxidative phosphorylation; PBS, phosphate buffered saline

Received 31 July 2018; revised 29 January 2019; accepted 4 February 2019; accepted manuscript published online 15 February 2019; corrected proof published online 23 April 2019

2016), suggesting that loss of epidermal stem cells contributes to skin aging. In fact, two possible pathways (not necessarily independent) by which NAD^+ might regulate aging have been proposed so far in tissues other than skin: (i) DNA repair and (ii) prevention of stem cell senescence. Insights have come from mouse models where two other NAD^+ precursors, nicotinamide mononucleotide and nicotinamide riboside, recently shown to be rapidly hydrolyzed to NAM in vivo after oral administration (Liu et al., 2018), also show anti-aging properties. With regard to DNA repair, PARP1 function and DNA repair efficiency decrease with age (Gorbunova et al., 2007; Grube and Burkle, 1992; Muiras et al., 1998) and, interestingly, nicotinamide mononucleotide treatment restores PARP1 activity in aged mice and correlates with reduced DNA damage in the liver after irradiation (Li et al., 2017). The mechanism by which NAD^+ enhances PARP1 activity has been described in details (Li et al., 2017) and it is now clear that maintenance of DNA repair can at least partly explain the anti-aging effect of NAD^+ in certain organs through maintenance of stem cell DNA integrity. With regard to senescence, nicotinamide riboside extends lifespan in mice and limits muscle, neural, and melanocyte stem cell senescence. This effect seems to occur through positive modulation of mitochondrial oxidative phosphorylation (OXPHOS) (Zhang et al., 2016), but how OXPHOS prevents stem cell senescence is yet to be determined. Moreover, NAM has recently been shown to increase lifespan of mesenchymal stem cells by delaying replicative senescence (Ok et al., 2018).

Loss of stem cell function can result from loss of DNA integrity and senescence, but also from differentiation. However, the role of NAM on adult tissue-specific stem cell terminal differentiation is not well understood. Strikingly, NAM helps maintain human embryonic stem cell and human induced pluripotent stem cell pluripotency, and improves human induced pluripotent stem cell reprogramming efficiency (Son et al., 2013). Interestingly, reprogramming to pluripotency is associated with a shift from OXPHOS to glycolysis (Folmes et al., 2011; Panopoulos et al., 2012), whereas embryonic stem cell differentiation correlates with increase in OXPHOS (Folmes et al., 2012). Therefore, modulating the major energy metabolism pathways (i.e., OXPHOS and glycolysis) might help control stem cell fate in terms of choice between stemness maintenance and differentiation. As these metabolic pathways rely on NAD^+, variations in NAD^+ levels may have a critical role in regulating stem cell fate and thus the stem cell pool. NAD^+ could be of particular importance in the renewal of the skin epidermis due to its reliance on stem cells. Indeed, upregulation of epidermal stem cell differentiation could lead to a loss of homeostasis that might contribute to skin aging.

Here, we used 3-dimensional (3D) organotypic models to show that high doses of NAM lead to epithelial thinning with loss of differentiation marker expression, yet remarkably proliferation is preserved. Using various 2-dimensional (2D) culture models, we show that low doses of NAM delay terminal differentiation of human primary keratinocytes (HPKs), while promoting a stem-like state and proliferation. By contrast, inhibiting NAMPT results in barely detectable levels of NAD^+ and massive HPK differentiation correlated with metabolic shutdown. Strikingly, HPK differentiation correlates with increased senescence, and both these phenotypes can be simultaneously rescued upon NAM addition. These results identify an intriguing link between a drop in metabolism consecutive to a lack of NAD^+, premature stem cell differentiation, and aging of the human skin.

RESULTS

High doses of NAM inhibit 3D organotypic HPK culture stratification

We first established MatTek 3D organotypic cultures to analyze the effects of NAM on the structure of a reconstituted skin epithelium. NAM was added 4 days after air-lift, and maintained in the medium during differentiation and stratification; the organotypic cultures were analyzed 12 days after air-lift. Low doses of NAM induced no obvious phenotype, but increasing doses led to a gradual thinning of the epithelium (Figure 1a, 1b, upper panels). Organotypic epidermal sections were labeled for the early differentiation marker keratin 10 expressed in suprabasal layers, and the late differentiation markers filaggrin and loricrin expressed in the granular upper layers. Here, we observed a dose-dependent loss of all differentiation markers tested, which were almost completely absent from epithelia 7 days after beginning of treatment with 15 mM NAM (Figure 1a, upper panel). Surprisingly, the Ki-67 proliferation marker remained strongly expressed in the basal layer, even at the highest dose of NAM, with no significant difference in the proportion of Ki-67−positive cells (Figure 1a, 1b). Proliferation was also investigated through a more functional assay based on BrdU incorporation in an independent experiment (Figure 1b). Again, we observed no significant difference in the proportion of BrdU-positive cells, except for a slight decrease with the highest dose of NAM, when expressed as a percentage of cells from the basal layer (Figure 1b, lower right panel). This unexpected finding in the context of epithelial thinning strongly suggests that this phenotype is due to a lack of differentiation rather than a lack of proliferation. In sum, we propose that the balance between HPK proliferation and differentiation in 3D models is modified by NAM.

NAM prevents HPK differentiation and enhances the clonogenicity and proportion of holoclones (HPK stem cells)

To further investigate the effects of NAM on HPK differentiation and proliferation, we treated 2D HPK cultures grown on 3T3-J2 feeders with low doses of NAM. High doses of NAM were not used due to the drastic effect on the structure of the epithelium in 3D organotypic cultures. HPKs were isolated from a fresh human skin biopsy and seeded on feeders, as described previously (Quek et al., 2018; Rheinwald and Green, 1975). The cells were then passaged and cultured for 5 days with or without 1 mM or 1.5 mM NAM. As expected from the results in organotypic cultures, reverse transcription quantitative PCR analyses of keratin 10, keratin 13, filaggrin, and involucrin showed that they were expressed at reduced levels after NAM treatment compared to untreated control cells (Figure 2a). We confirmed this repression of differentiation at the protein level by Western blotting (Figure 2b). Interestingly, repressed HPK differentiation was maintained and even amplified over time, as the expression of differentiation markers increased in control cells over a period of 12 days without passaging (Figure 2c). A range of NAM

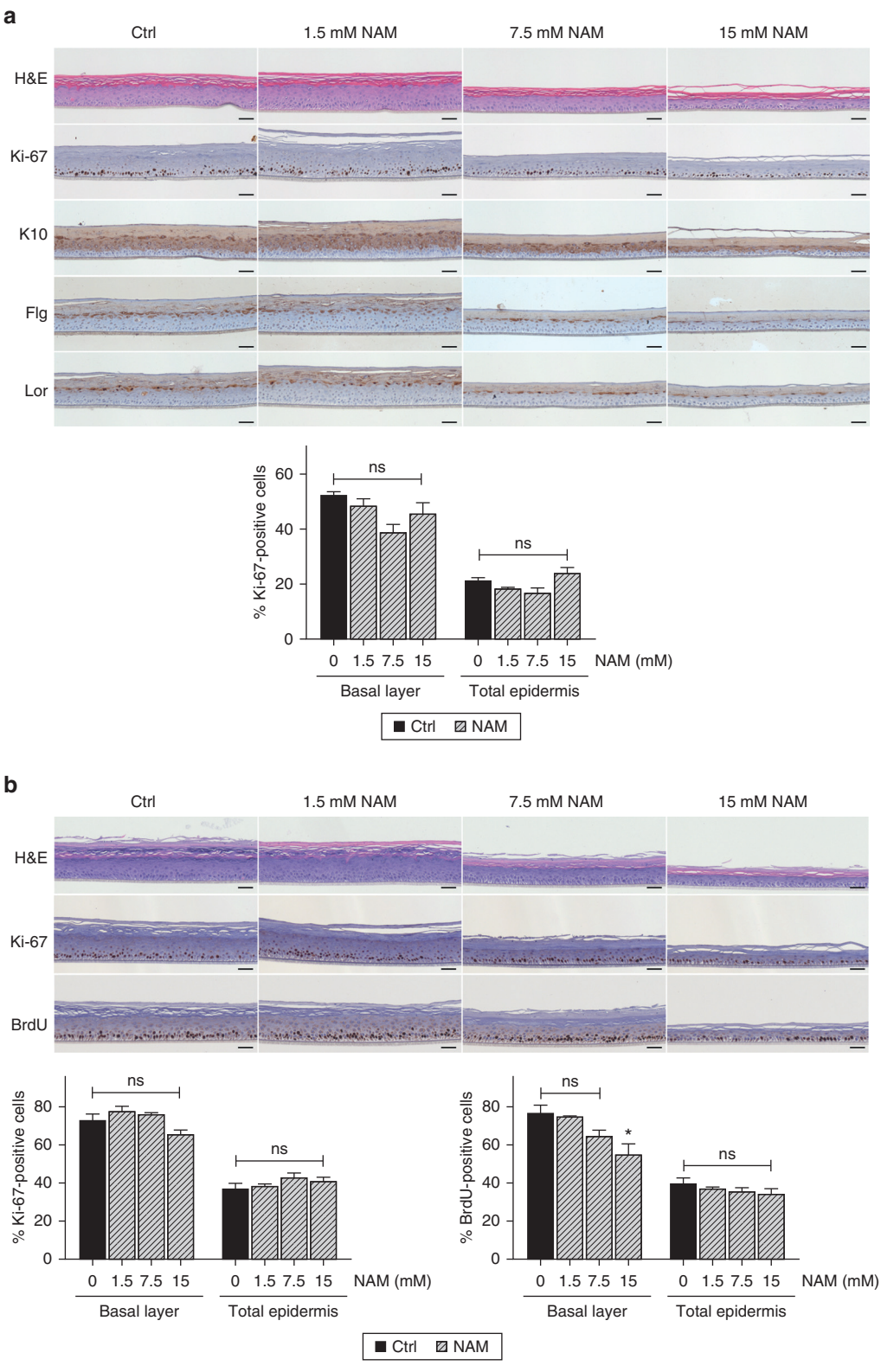

Figure 1. High doses of NAM inhibit stratification of 3-dimensional organotypic human primary keratinocyte cultures. (**a**) Upper panel: Human primary keratinocyte cultures were grown to a full thickness epithelium with or without the indicated doses of NAM. H&E and immunohistochemistry were performed. Scale bar = 50 μm. Lower panel: Ki-67−positive cells were quantified as the percentages of cells from the basal layer or from the total epidermis. (**b**) Upper panel: Another batch of 3D cultures was used to perform BrdU incorporation. Scale bar = 50 μm. Lower panel: Both BrdU-positive and Ki-67−positive cells were quantified as in (**a**). For (**a**) and (**b**), three to six fields were analyzed per condition (200−600 cells per field). Statistical analyses: one-way analysis of variance, $n \geq 3$. Ctrl, untreated control cells; H&E, hematoxylin and eosin; K10, keratin 10; Flg, filaggrin; Lor, loricrin; NAM, nicotinamide; ns, not significant.

concentrations was assessed (from 0.1 mM to 2 mM), and although the effect of NAM on differentiation was significant for most of the genes from 0.5 mM (Supplementary Figure S1 online), it was most pronounced with 1−2 mM NAM. Importantly, while the fasting NAM plasma concentration in humans ranges from 213 nM to 340 nM (Catz et al., 2005; Jacobson et al., 1995), NAM plasma concentrations between 0.5 mM and 1.5 mM have been reported after oral administration of 4 g NAM, corresponding to a dose of 60 mg/kg (Bussink et al., 2002; Stratford et al., 1992). Therefore, the NAM concentrations used here fall within the range of NAM plasma concentrations achieved after oral intake of NAM.

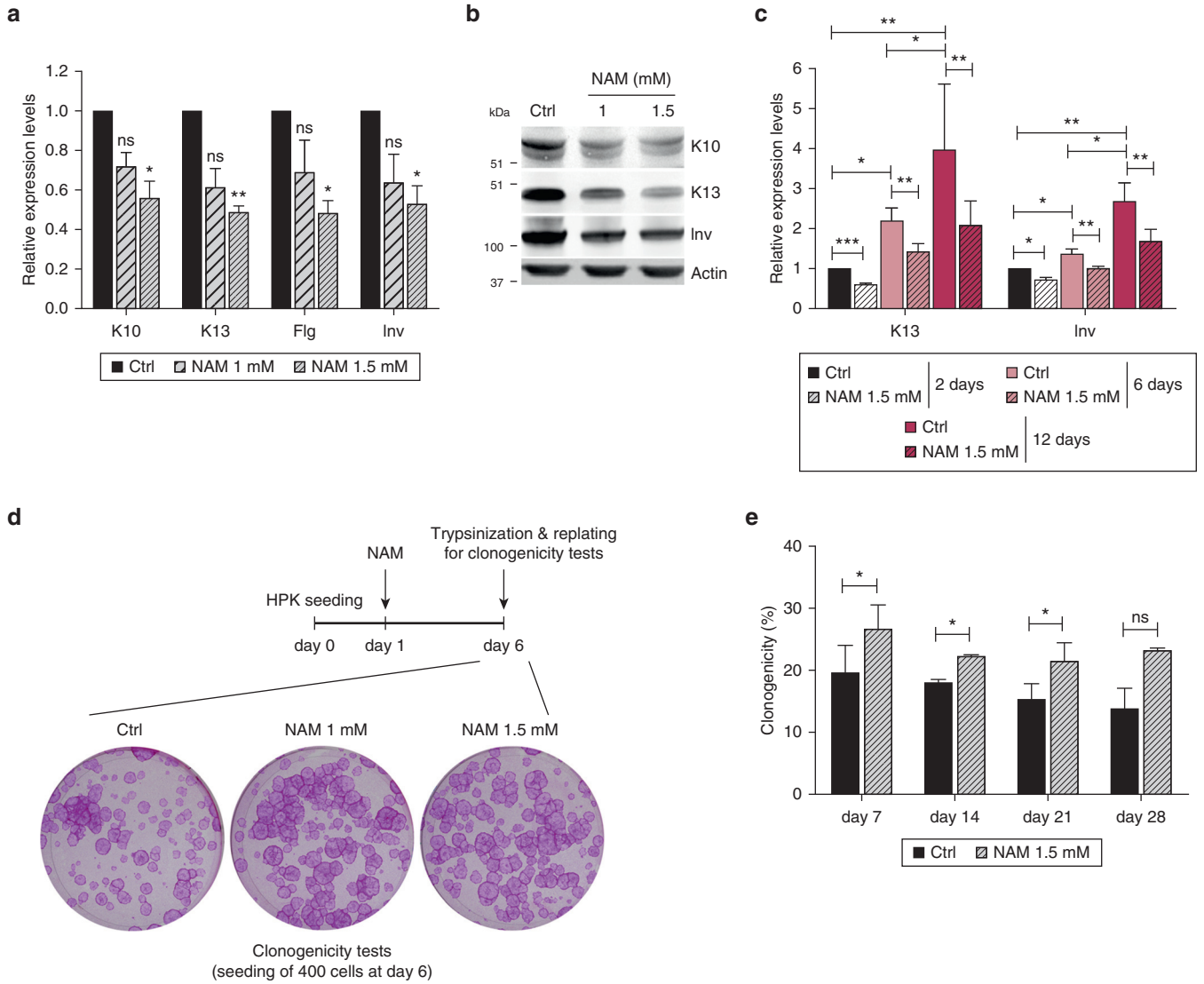

Figure 2. NAM prevents human primary keratinocyte differentiation and enhances both the clonogenicity and the proportion of holoclones. (**a**) Reverse transcription quantitative PCR analyses after treatment of human primary keratinocyte (grown on 3T3-J2 feeders) as indicated. Statistical analyses: one sample *t* tests with a hypothetical value of 1, n = 3. (**b**) Western blot analyses after treatment as in (**a**). (**c**) Reverse transcription quantitative PCR analyses after treatment as indicated. Statistical analyses: paired *t* tests, n = 5. (**d**) Clonogenicity tests performed without treatment (Ctrl) or after 5 days of 1 mM or 1.5 mM NAM treatment. (**e**) Quantifications of clonogenicity tests performed after 7, 14, 21, or 28 days of 1.5 mM NAM treatment. Statistical analyses: paired *t* tests, n = 3. Ctrl, untreated control cells, K10, keratin 10; K13, keratin 13; Flg, filaggrin; Inv, involucrin; NAM, nicotinamide; ns, not significant.

We next performed clonogenicity analyses of the cells after treatment with low doses of NAM. Here, we assessed the proportions of: (i) keratinocyte stem cells (holoclones), known to proliferate and give rise to large colonies containing mostly small keratinocytes; (ii) cells committed to imminent differentiation with weak proliferative capability (paraclones) that generate either no or small colonies containing mostly large differentiated cells; (iii) cells with intermediate proliferative capabilities (meroclones), which have been referred to as progenitors or early-stage transient amplifying cells, although some of them can be stem cells (Barrandon and Green, 1987; Beaver et al., 2014). Clonogenicity tests after 5 days of NAM treatment showed that NAM enhanced both the number of colonies and the proportion of holoclones compared to untreated cells (Figure 2d).

To determine the long-term effects of NAM, we passaged HPKs every 7 days for 28 days (with or without NAM) and performed clonogenicity tests at each passage (Supplementary Figure S2a online). We found long-term maintenance of the enhanced clonogenicity in the NAM-treated population (Figure 2e). This finding was further supported by the repression of differentiation markers over time (Supplementary Figure S2b). Moreover, similar to day 6 (Figure 2d), the ratio of "growing" (holoclones + meroclones) versus "non-growing" (paraclones) colonies shifted in favor of the growing colonies, with ~20% increase compared to untreated control cells at day 7 (Supplementary Figure S2c). Nevertheless, from day 21 onward, although the effect on clonogenicity was maintained (Figure 2e), a decline in the proportion of growing colonies occurred (Supplementary Figure S2c). At day 28, the repression of differentiation markers, although still visible, became nonsignificant except for Keratin 13 (Supplementary Figure S2b). In conclusion,

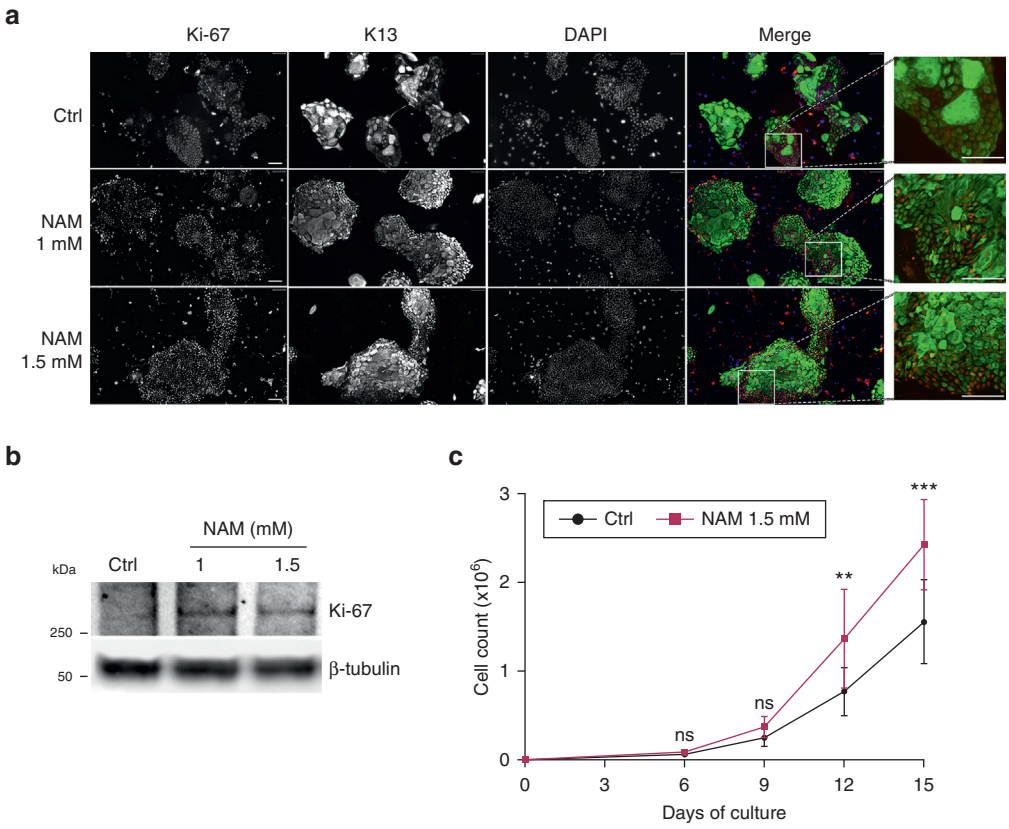

Figure 3. NAM upregulates human primary keratinocyte proliferation in 2-dimensional cultures. (**a**) Immunofluorescence analyses of the Ki-67 proliferation marker and the K13 differentiation marker after human primary keratinocyte treatment with 1 or 1.5 mM NAM for 5 days. The white boxes correspond to areas magnified on the right panels. Scale bar = 100 μm. (**b**) Western blot analyses of the Ki-67 proliferation marker expression in cells treated as in (**a**). (**c**) Proliferation curves showing the total cell counts of cells treated as indicated for 3, 6, 9, 12, or 15 days. Statistical analyses: two-way analysis of variance, n = 4. Ctrl, untreated control cells; K13, keratin 13; NAM, nicotinamide; ns, not significant.

NAM maintains a constant clonogenicity over a period of 4 weeks (28 days) in culture. Nevertheless, the stem cell pool, although higher the first 2 weeks, seems to decrease later.

NAM upregulates HPK proliferation in 2D cultures

Our data so far indicated that 3D cultures did not show an increase in proliferation after NAM treatment (Figure 1), yet the clonogenicity improved in 2D cultures (Figure 2d, 2e). We hypothesized that inhibited differentiation upon NAM treatment in 2D cultures may be coupled with an increase in global proliferation (that is too low to be observed or absent in 3D cultures), and possibly an increase in stemness of the population, given that the proportion of holoclones increased the first 2 weeks. To test our hypothesis, we treated 2D cultures with NAM for 5 days and analyzed Ki-67 proliferation marker expression. Treatment with 1 mM and 1.5 mM NAM induced HPK proliferation, as evidenced by enhanced Ki-67 expression at the protein level (Figure 3a, 3b). Immunofluorescence studies showed that not only were more cells positive for Ki-67, but these positive cells were typically brighter and smaller than positive cells in the control group. In addition, the NAM-treated culture seemed to adopt a multilayered structure, which was a recurrent finding in all our experiments, and is in agreement with enhanced proliferation and reduced differentiation of HPKs (Figure 3a, magnified images).

To check whether this induction of proliferation was sustained over time, we generated proliferation curves over a period of 15 days. Here, the total cell count noticeably increased in the NAM-treated population compared to the control population from day 9, reached significantly higher levels from day 12, and reached maximal significance by day 15 (Figure 3c). In fact, some experiments showed up to twice the number of cells in the NAM-treated population compared to the control population at day 15. Taken together, these data support that NAM induces long-term up-regulation of proliferation in HPK 2D cultures.

Inhibition of NAM conversion to NAD^+ induces HPK differentiation

As expected regarding the known role of NAM as a precursor of NAD^+, we found that after 2 days of treatment, intracellular NAD^+ levels were higher in NAM-treated cells than in untreated control cells (Figure 4a). We considered, therefore, that the effect of NAM on differentiation was likely due to its conversion to NAD^+. However, adverse effects of NAM have been reported, which might contribute to the phenotypes we observed in our cultures. Indeed, at least in vitro, NAM is an inhibitor of several enzymes that require NAD^+ to function, in particular SIRT1 that promotes HPK differentiation (Blander et al., 2009). Therefore, we established a reverse experiment, whereby we analyzed HPK differentiation in response to NAD^+ depletion by exposing cells to FK866. This drug inhibits the NAMPT enzyme and prevents the conversion of NAM into NAD^+ through the salvage pathway. Strikingly, 0.1 μM FK866 treatment did not induce any phenotype after 1 day, despite a drop of NAD^+, but massive differentiation concomitant with a dramatic drop in NAD^+ levels was evident after 2 days (Figure 4a, 4b). This effect was accompanied by flatter cell shape and an increase in cell size

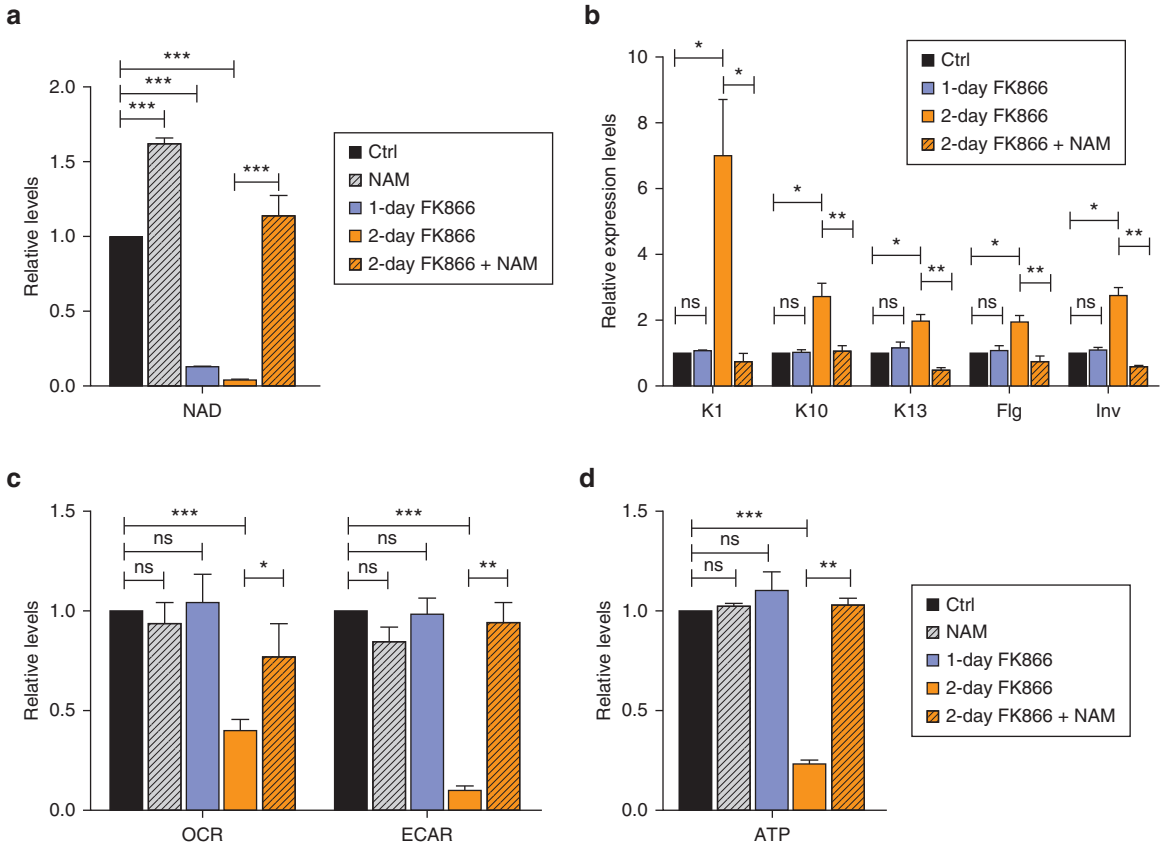

Figure 4. Inhibition of NAM conversion to NAD^+ in human primary keratinocytes induces differentiation and a drop in metabolic activity. (**a**) NAD^+/NADH quantification (NAD) in human primary keratinocytes treated as indicated (0.1 μM FK866 and/or 1.5 mM NAM). For co-treatment, the two compounds were added simultaneously 2 days before quantification. Statistical analyses: paired *t* tests, n = 4. (**b**) Reverse transcription quantitative PCR analyses after treatment as indicated. Statistical analyses: paired *t* tests, n = 3. (**c**) Basal levels of oxidative phosphorylation (OCR) and glycolysis (ECAR) in cells treated as in (a). Statistical analyses: paired *t* tests, n ≥ 4. (**d**) ATP levels in cells treated as in (**a**). Statistical analyses: paired *t* tests, n = 4. ATP, adenosine triphosphate; Ctrl, untreated control cells; ECAR, extracellular acidification rate; Flg, filaggrin; Inv, involucrin; K1, keratin 1; K10, keratin 10; K13, keratin 13; NAM, nicotinamide; OCR, oxygen consumption rate; ns, not significant.

(Supplementary Figure S3a online), indicative of differentiation. Finally, to confirm that the effect of FK866 was due to the lack of NAD^+ and not due to an off-target effect of the drug, we down-regulated NAMPT by small interfering RNA and observed that HPK differentiation was induced (Supplementary Figure S3b).

Crystal structure analyses have determined that NAM and FK866 compete to bind NAMPT (Khan et al., 2006). We therefore assumed that combined exposure to NAM and FK866 should restore NAD^+ levels and prevent the differentiation phenotype if differentiation was indeed induced by the lack of NAD^+. As expected, combined treatment with 0.1 μM FK866 (shown above to induce differentiation) and 1.5 mM NAM prevented the drop in NAD^+ levels and the differentiation phenotype (Figure 4a, 4b, Supplementary Figure S3a). Altogether, these data indicate that a lack of NAD^+ induces HPK differentiation, and that NAM mainly exerts its anti-differentiative effects by maintaining the NAD^+ pool.

Inhibition of NAM conversion to NAD^+ reduces the rates of glycolysis and OXPHOS

NAD^+ and NADH have a central role in metabolism, especially during OXPHOS and glycolysis. As such, we monitored these two pathways using the Seahorse XFe24 Analyzer. Similar to our results regarding cellular differentiation, treatment with 0.1 μM FK866 for 1 day did not induce any significant metabolic phenotype (Figure 4c). This finding may be because depletion of the NAD^+ pool did not reach a critical level or because the metabolic response was not immediate. After 2 days of FK866 treatment, we detected a partial shutdown of OXPHOS (measured by the oxygen consumption rate) by ~55% together with ~90% inhibition of glycolysis (measured by the extracellular acidification rate) (Figure 4c). This effect correlated with a ~75% drop in adenosine triphosphate (ATP) levels (Figure 4d). Importantly, co-treatment with 1.5 mM NAM rescued the ATP, OXPHOS, and glycolysis rates back to levels detected in the control population (Figure 4c, d). These experiments unambiguously link NAD^+ depletion and reduced metabolic capacity to enhanced differentiation of HPKs.

As FK866 induces cell death in numerous cancer cell lines, we performed Annexin V staining and analyzed the results by flow cytometry. We found no increase in apoptosis in FK866-treated cells after 1 or 2 days compared to control cells, demonstrating that the drop of ATP and modulation of OXPHOS and glycolysis were not associated with apoptosis (Supplementary Figure S4 online).

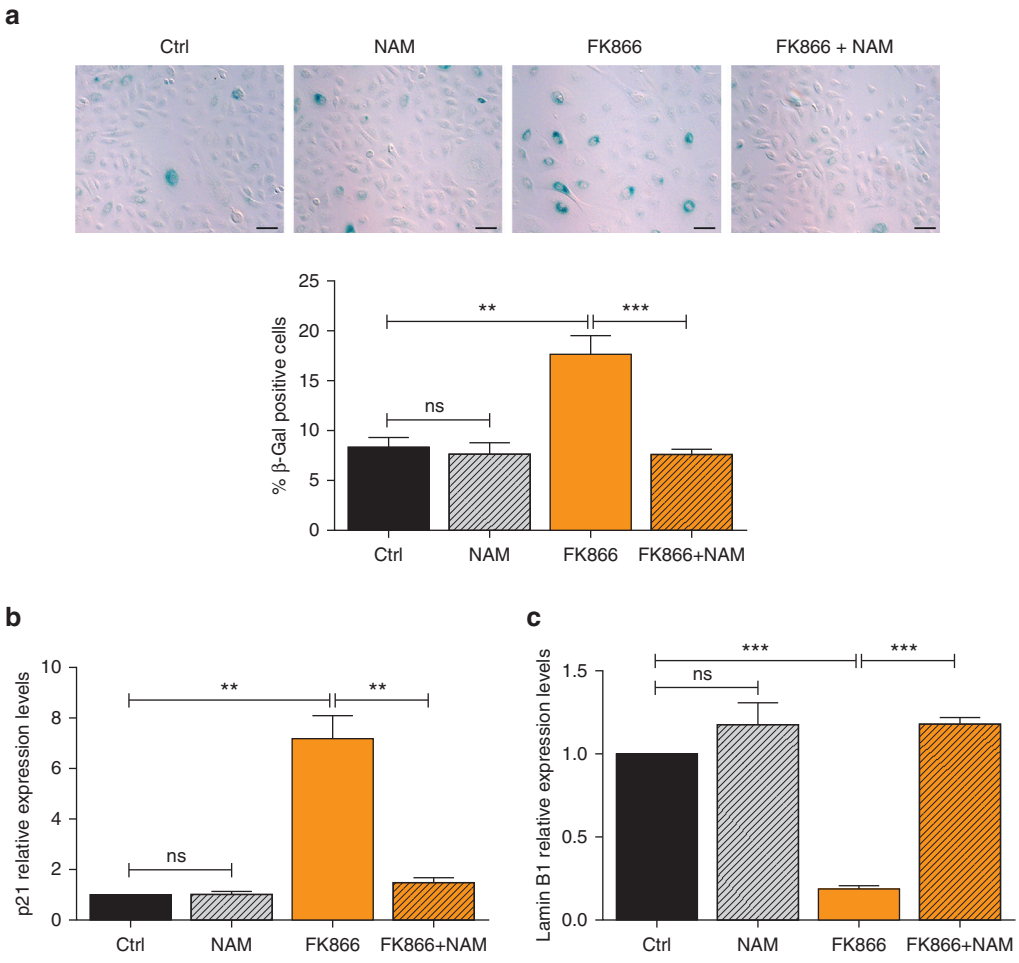

Figure 5. Inhibition of NAM conversion to NAD^+ induces human primary keratinocyte senescence. (**a**) Upper panel: β-Gal staining of human primary keratinocytes treated as indicated. Untreated human primary keratinocytes were used as a negative control. Scale bar = 50 μm. Lower panel: Quantification of β-gal −positive cells in the populations, n ≥ 300 cells for each condition. Statistical analyses: one-way analysis of variance, n = 3. (**b**) Reverse transcription quantitative PCR analyses of p21 expression in cells treated as in (**a**). (**c**) Reverse transcription quantitative PCR analyses of lamin B1 expression in cells treated as in (**a**). Statistical analyses for (**b**) and (**c**): paired *t* tests, n ≥ 3. Ctrl, untreated control cells; β-Gal, β-galactosidase; NAM, nicotinamide; ns, not significant.

Increased HPK differentiation after NAD^+ depletion correlates with a senescent phenotype

The levels of NAD^+ decrease in aging cells (Camacho-Pereira et al., 2016; Massudi et al., 2012; Yoshino et al., 2011). As such, we studied senescence levels in HPKs treated with FK866, with or without NAM. FK866-treated cells showed a marked increase in β-galactosidase staining compared to untreated cells (Figure 5a), a strong increase in p21 (Figure 5b) and a drop in lamin B1 expression (Figure 5c)—a protein shown to be lost during senescence (Dreesen et al., 2013). Interestingly p16 was not significantly modulated (Supplementary Figure S5 online). These data indicate that FK866 induces both differentiation and senescence. As before, NAM could almost completely prevent senescence, as visualized by a reduced proportion of β-galactosidase−positive cells compared to cells treated with FK866 alone, and by the rescue of p21 and lamin B1 mRNA expression levels after 2 days of treatment (Figure 5a−5c).

DISCUSSION

Our study has shown that NAM prevents premature differentiation in HPKs lacking NAD^+. Under normal conditions, NAM delays differentiation of HPKs in culture over time, and we hypothesize that this differentiation might occur as a consequence of lack of NAM in the media, as commercial media used here contain a low amount of NAM (ranging from 0.3 to 22 μM). Not only is NAM able to prevent HPK differentiation, but it can shift the balance between proliferation and differentiation toward proliferation in 2D culture models. This effect might help maintain a higher number of stem cells over time, as shown in our clonogenicity assays. In our 3D models, the main phenotype observed after NAM treatment was an inhibition of differentiation and there was little effect on proliferation. As such, we propose that in 3D organotypic cultures, which are physiologically much closer to the skin epithelium than 2D models, stem cells may be in a more quiescent state than in 2D cultures, where they are known to readily proliferate. This phenomenon may explain the difficulties in observing a significant increase in the number of dividing cells in the basal layer.

Interestingly, induced differentiation after NAD^+ depletion was associated with premature senescence, and both phenotypes could be concurrently rescued by exogenous addition of NAM. Regarding the underlying mechanisms, the consequences of a lack of NAD^+ are complex as NAD^+ has major roles in both DNA repair and metabolism (Canto et al., 2015). We showed that the massive loss of glycolysis (and the moderate suppression of OXPHOS) after FK866 treatment could be successfully rescued by NAM. These data led us to conclude that a lack of NAD^+ drives a drop in metabolism (namely glycolysis) in HPKs, which is likely to induce both the differentiation and senescent phenotypes observed. Hence, as is known to be the case in embryonic stem cells and in most tissue-specific stem cells, HPK stemness could

rely on glycolysis and, therefore, preserving this glycolysis pathway may be key to preventing premature differentiation in the adult epidermis (Shyh-Chang et al., 2013; Zhang et al., 2018). With regard to senescence, senescent fibroblasts in culture are typically more glycolytic than non-senescent cells (Bittles and Harper, 1984; Wiley and Campisi, 2016), and OXPHOS activity seems important in preventing senescence (Wiley et al., 2016). Therefore, it may be conceivable that the 55% reduction in OXPHOS observed after FK866 treatment drives senescence of HPK stem cells, even in the absence of glycolysis. However, it is also possible that the senescence observed here occurs after differentiation. Indeed, terminally differentiated post-mitotic cells, such as adipocytes, cardiac myocytes, and neurons, adopt characteristics of senescent cells in several diseases (Naylor et al., 2013). This phenomenon has been termed *senescence after differentiation* and could participate in the aging process. Although more work is needed to understand whether the population of "aging" cells observed here after FK866 treatment corresponds to senescent HPK stem cells, senescent differentiated cells, or a mixture of both, our work firmly establishes a link between NAD^+ levels, differentiation, and senescence in skin epidermis.

As the NAD^+ pool depletes with cell aging (Camacho-Pereira et al., 2016; Massudi et al., 2012; Yoshino et al., 2011) and is expected to deplete faster with photoexposure, given the role of NAD^+ in DNA repair, our study raises the intriguing possibility that premature aging in skin is driven at least in part, by the loss of keratinocyte stem cells due to differentiation. A separate finding to this study is that NAM is a useful medium supplement during in vitro HPK expansion to prevent stem cell differentiation and preserve the stem cell and/or progenitor pool. This experimental finding may be particularly valuable during HPK expansion in culture before skin grafting of severe burn patients—a process during which the known high loss of stem cells limits the engraftment success rate.

MATERIALS AND METHODS

Study approval

This study was approved by the National University of Singapore Institutional Review Board (NUS-IRB reference code: B-14-257E).

Isolation of primary keratinocytes from human skin

HPKs were obtained from healthy human skin samples (upper limb, 41-year-old female donor) from de-identified surplus surgical waste with written informed patient consent and ethical clearance. HPKs were isolated as described previously (Quek et al., 2018).

HPK culture, growth curves, and clonogenicity tests

HPKs were cultured on lethally irradiated murine 3T3-J2 feeder cells in cFAD medium (3:1 DMEM/Ham's F-12) supplemented with 10% fetal calf serum, 1% penicillin/streptomycin, and 10 ng/ml epidermal growth factor (Rheinwald and Green, 1975; Simon and Green, 1985). The medium was replaced every 2–3 days. For metabolism experiments, HPKs were cultured in a feeder-free system with Dermalife medium (LL-0007; Lifeline Cell Technology, Oceanside, CA). FK866 (F8557; Sigma Aldrich, St-Louis, MO) was used at a dose of 0.1 μM.

To establish growth curves, HPKs were plated at low density (300 cells) and cultured in cFAD/fetal calf serum on feeders.

Clonogenicity assays were performed by seeding 400 HPKs on feeders on 10-cm dishes. The cells were grown for 12 days (without NAM) before staining with 1% Rhodamine B (JT Baker U872; Avantor Performance Materials, Center Valley, PA). Colonies were manually quantitated under a Stemi 2000C Stereomicroscope (Zeiss, Oberkochen, Germany).

Reverse transcription quantitative PCR

Total RNA was extracted using an RNeasy Mini Kit (Qiagen, Hilden, Germany) and treated with DNase I. Isolated RNA (2.5 μg) was used for reverse transcription using Superscript II (Invitrogen, Carlsbad, CA) according to the manufacturer's instructions. Quantitative PCR analyses were carried out as described previously (Thierry et al., 2004). Amplification values were normalized to the TATA-binding protein cDNA. Primers used are shown in Supplementary Table S1 online.

Immunofluorescence

HPKs grown on feeders were cultured on glass slides, fixed, and permeabilized with ice-cold acetone/methanol (1:1) for 7 minutes at −20°C, and blocked with phosphate buffered saline (PBS)/2% serum. Cells were then incubated with primary antibodies (Supplementary Table S2 online) followed by washing and incubation with secondary antibodies (Alexa Fluor, ThermoFisher Scientific, Waltham, MA) and DAPI (1 μg/ml) before mounting (Hydromount; National Diagnostics, Atlanta, GA). Images were captured with a Zeiss AxioImager Z1 microscope and analyzed using Zen 2 software (Zeiss).

Protein extraction and Western blotting

Protein extraction and Western blotting were performed as described previously (Quek et al., 2018). Primary antibodies used are detailed in Supplementary Table S2.

Glycolysis (extracellular acidification rate), OXPHOS (oxygen consumption rate), ATP, and NAD^+/NADH measurements

The basal oxygen consumption rate, as a measure of OXPHOS, and extracellular acidification rate, as a measure of glycolysis, were measured using the Seahorse XFe 24 Analyzer (Agilent, Santa Clara, CA). Prior to measurements, the growth medium was changed to a custom-made EpiLife medium (Life Technologies, Carlsbad, CA) containing no calcium, D-glucose, HEPES, L-glutamine, phenol red, sodium bicarbonate, or sodium pyruvate. Sodium pyruvate (1 mM), glutamine (6 mM), insulin (10 μg/ml), and glucose (10 mM, only added when the XF Cell Mito Stress Test Kit was used; Agilent, Santa Clara, CA) were added to the medium prior to experiments. The cells were incubated at 37°C in a CO_2-free incubator for 1 hour prior to measurements. The Seahorse XF Cell Mito Stress Test Kit (103015-100) and Seahorse XF Glycolysis Stress Test Kit (103020-100, Agilent, Santa Clara, CA) were used following the manufacturer's instructions. Only basal levels are shown.

NAD^+/NADH measurements were performed using the NAD/NADH Assay Kit (600480; Cayman Chemical, Ann Arbor, MI).

ATP measurements were recorded by CellTiter-Glo Luminescence Cell Viability Assay (G7570; Promega, Madison, WI), following the manufacturer's instructions.

Crystal Violet staining and quantification

Raw oxygen consumption rate, extracellular acidification rate, ATP, and NAD^+/NADH values were normalized using Crystal Violet (C3886; Sigma Aldrich, St, MO). The cells were fixed with 4% paraformaldehyde for 15 minutes at room temperature and then washed with PBS, followed by water, before addition of 0.1% Crystal

Violet for 15 minutes at room temperature. After two washes with water, the Crystal Violet stain was eluted in 10% acetic acid and the absorbance was measured at 590 nm (SpectraMax M5 Microplate Reader; Molecular Devices, San Jose, CA).

β-Galactosidase assay

HPKs were cultured on glass coverslips and analyzed for β-galactosidase activity using the Senescence β-Galactosidase Staining Kit (9860; Cell Signaling Technology, Danvers, MA), following the manufacturer's recommendations. Images were captured with an AxioImager Z1 (Zeiss) using a 20× Plan Apochromatic objective lens. Blue senescent cells and non-blue cells were counted manually.

3D organotypic skin epidermis culture

A human epidermis model (EpiDerm-200-3S; MatTek Corporation, Ashland, MA) derived from newborn foreskin was used to assay the effects of NAM on 3D organotypic models. Briefly, cells received as a monolayer were stratified to full thickness according to the manufacturer's instructions, in a humidified atmosphere with 5% CO_2 at 37°C. Tissues were harvested on day 12, fixed in 10% neutral buffered formalin for 4 hours, and then processed into wax blocks before further analyses.

Immunohistochemistry on 3D organotypic sections

Paraffin samples were dewaxed in xylene and rehydrated through a descending ethanol to water series (3 minutes per solution). Epitope retrieval was performed at 121°C for 10 minutes using Citrate Buffer pH 6.0 Antigen Retriever (64142; Electron Microscopy Sciences, Hatfield, PA), and the slides were cooled prior to three washes in PBS/0.05% Tween 20. The sections were then incubated with water/1% H_2O_2 for 30 minutes to block endogenous peroxidase, rinsed with water and PBS/0.05% Tween 20 for 5 minutes, and incubated with PBS/10% goat serum (Dako, Glostrup, Denmark) for 20 minutes before exposure to primary antibodies (Supplementary Table S2) overnight at 4°C. Samples were thoroughly washed with water for 10 minutes and PBS/0.05% Tween 20 for 5 minutes followed by 30-minute incubation with EnVision+ System-horseradish peroxidase–labeled polymer anti-mouse antibody (K4001; Dako, Carpinteria, CA). Then, the samples were washed in water and PBS before incubation with Liquid DAB+ Substrate Chromogen System (K3468; Dako), for 3–5 minutes. The reaction was stopped by rinsing in tap water, and sections were counterstained in Mayer's hematoxylin for 3–5 minutes, rinsed in tap water for 1 minute and in Scott's bluing water for 2 minutes. Finally, the sections were dehydrated in graded ethanol, cleared in xylene, and mounted in Cytoseal 60 (ThermoScientific, Waltham, MA).

BrdU incorporation assay in 3D organotypic culture

BrdU (Abcam, Cambridge, UK) at 10 μM final concentration was added to the culture medium 16 hours before fixation. BrdU incorporation was detected using a BrdU immunohistochemistry kit (ab125306; Abcam) following manufacturer's recommendations. The samples were incubated with DAB for 5 minutes, followed by hematoxylin counterstain. Images were acquired on the AxioImager Z1 (Zeiss) using the ×20 Plan Apochromatic objective lens. The BrdU-positive nuclei and total number of nuclei (DAPI stained) were counted manually.

Statistical analyses

Statistical analyses were performed using GraphPad Prism, version 5.03 (GraphPad, San Diego, CA), with one-way analysis of variance, two-way analysis of variance, or *t* test as indicated ($^*P < 0.05$; $^{**}P < 0.01$; $^{***}P < 0.001$; ns = not significant). All data represent the mean ± standard error of the mean.

Data availability statement

Data sharing is not applicable to this article as no data sets were generated or analyzed during the current study.

ORCIDs

Chye ling Tan: https://orcid.org/0000-0001-7688-1316
Toby Chin: https://orcid.org/0000-0003-0025-7992
Christina Yan Ru Tan: https://orcid.org/0000-0003-1901-5934
Holly A Rovito: https://orcid.org/0000-0003-2352-1477
Ling Shih Quek: https://orcid.org/0000-0002-3861-8901
John Oblong: https://orcid.org/0000-0001-7628-6242
Sophie Bellanger: https://orcid.org/0000-0002-0689-2201

CONFLICTS OF INTEREST

JEO and HAR are full-time employees of The Procter & Gamble Company (Cincinnati, OH). The remaining authors state no conflict of interest.

ACKNOWLEDGMENTS

The authors would like to thank all the patients for participating in this study, as well as the Skin Cell Bank and Kathi Mujynya for providing the HPKs cells. They are also grateful to Yann Barrandon for providing the 3T3-J2 cells. The authors also thank Jessica Tamanini of Insight Editing London for English language editing of this manuscript prior to submission. This study was supported by the Agency for Science Technology and Research (A*STAR) and The Procter & Gamble Company.

AUTHOR CONTRIBUTIONS

Conceptualization: SB, JEO. Formal analysis: CLT, TC, CYRT, SB. Funding acquisition: SB, JEO. Investigation: CLT, TC, CYRT, LSQ. Methodology: CLT, TC, CYRT, HAR. Project administration: SB, JEO. Resources: TC, LSQ. Supervision: SB, JEO. Visualization: SB. Writing, original draft preparation: SB. Writing, review and editing: SB, JEO, CLT, CYRT.

SUPPLEMENTARY MATERIAL

Supplementary material is linked to the online version of the paper at www.jidonline.org, and at https://doi.org/10.1016/j.jid.2019.02.005.

REFERENCES

Barrandon Y, Green H. Three clonal types of keratinocyte with different capacities for multiplication. Proc Natl Acad Sci USA 1987;84:2302–6.

Beaver CM, Ahmed A, Masters JR. Clonogenicity: holoclones and meroclones contain stem cells. PLoS One 2014;9:e89834.

Bissett DL, Miyamoto K, Sun P, Li J, Berge CA. Topical niacinamide reduces yellowing, wrinkling, red blotchiness, and hyperpigmented spots in aging facial skin. Int J Cosmet Sci 2004;26:231–8.

Bissett DL, Oblong JE, Berge CA. Niacinamide: A B vitamin that improves aging facial skin appearance. Dermatol Surg 2005;31(7 Pt 2):860–5; discussion 865.

Bittles AH, Harper N. Increased glycolysis in ageing cultured human diploid fibroblasts. Biosci Rep 1984;4:751–6.

Blander G, Bhimavarapu A, Mammone T, Maes D, Elliston K, Reich C, et al. SIRT1 promotes differentiation of normal human keratinocytes. J Invest Dermatol 2009;129:41–9.

Bussink J, Stratford MR, van der Kogel AJ, Folkes LK, Kaanders JH. Pharmacology and toxicity of nicotinamide combined with domperidone during fractionated radiotherapy. Radiother Oncol 2002;63:285–91.

Camacho-Pereira J, Tarrago MG, Chini CCS, Nin V, Escande C, Warner GM, et al. CD38 Dictates age-related NAD decline and mitochondrial dysfunction through an SIRT3-dependent mechanism. Cell Metab 2016;23:1127–39.

Canto C, Menzies KJ, Auwerx J. NAD(+) metabolism and the control of energy homeostasis: a balancing act between mitochondria and the nucleus. Cell Metab 2015;22:31–53.

Catz P, Shinn W, Kapetanovic IM, Kim H, Kim M, Jacobson EL, et al. Simultaneous determination of myristyl nicotinate, nicotinic acid, and nicotinamide in rabbit plasma by liquid chromatography-tandem mass spectrometry using methyl ethyl ketone as a deproteinization solvent. J Chromatogr B Analyt Technol Biomed Life Sci 2005;829:123–35.

Chen AC, Martin AJ, Choy B, Fernandez-Penas P, Dalziell RA, McKenzie CA, et al. A phase 3 randomized trial of nicotinamide for skin-cancer chemoprevention. N Engl J Med 2015;373:1618–26.

Chini CCS, Tarrago MG, Chini EN. NAD and the aging process: role in life, death and everything in between. Mol Cell Endocrinol 2017;455:62–74.

Damian DL, Patterson CR, Stapelberg M, Park J, Barnetson RS, Halliday GM. UV radiation-induced immunosuppression is greater in men and prevented by topical nicotinamide. J Invest Dermatol 2008;128:447–54.

Dreesen O, Chojnowski A, Ong PF, Zhao TY, Common JE, Lunny D, et al. Lamin B1 fluctuations have differential effects on cellular proliferation and senescence. J Cell Biol 2013;200:605–17.

Fivenson DP, Breneman DL, Rosen GB, Hersh CS, Cardone S, Mutasim D. Nicotinamide and tetracycline therapy of bullous pemphigoid. Arch Dermatol 1994;130:753–8.

Folmes CD, Dzeja PP, Nelson TJ, Terzic A. Metabolic plasticity in stem cell homeostasis and differentiation. Cell Stem Cell 2012;11:596–606.

Folmes CD, Nelson TJ, Martinez-Fernandez A, Arrell DK, Lindor JZ, Dzeja PP, et al. Somatic oxidative bioenergetics transitions into pluripotency-dependent glycolysis to facilitate nuclear reprogramming. Cell Metab 2011;14:264–71.

Garten A, Schuster S, Penke M, Gorski T, de Giorgis T, Kiess W. Physiological and pathophysiological roles of NAMPT and NAD metabolism. Nat Rev Endocrinol 2015;11:535–46.

Gensler HL. Prevention of photoimmunosuppression and photocarcinogenesis by topical nicotinamide. Nutr Cancer 1997;29:157–62.

Giangreco A, Qin M, Pintar JE, Watt FM. Epidermal stem cells are retained in vivo throughout skin aging. Aging Cell 2008;7:250–9.

Gorbunova V, Seluanov A, Mao Z, Hine C. Changes in DNA repair during aging. Nucleic Acids Res 2007;35:7466–74.

Grube K, Burkle A. Poly(ADP-ribose) polymerase activity in mononuclear leukocytes of 13 mammalian species correlates with species-specific life span. Proc Natl Acad Sci USA 1992;89:11759–63.

Imai SI, Guarente L. It takes two to tango: NAD(+) and sirtuins in aging/longevity control. NPJ Aging Mech Dis 2016;2:16017.

Jacobson EL, Dame AJ, Pyrek JS, Jacobson MK. Evaluating the role of niacin in human carcinogenesis. Biochimie 1995;77:394–8.

Jones DL, Rando TA. Emerging models and paradigms for stem cell ageing. Nat Cell Biol 2011;13:506–12.

Keyes BE, Fuchs E. Stem cells: aging and transcriptional fingerprints. J Cell Biol 2018;217:79–92.

Khan JA, Tao X, Tong L. Molecular basis for the inhibition of human NMPRTase, a novel target for anticancer agents. Nat Struct Mol Biol 2006;13:582–8.

Kim B, Halliday GM, Damian DL. Oral nicotinamide and actinic keratosis: a supplement success story. Curr Probl Dermatol 2015;46:143–9.

Levine D, Even-Chen Z, Lipets I, Pritulo OA, Svyatenko TV, Andrashko Y, et al. Pilot, multicenter, double-blind, randomized placebo-controlled bilateral comparative study of a combination of calcipotriene and nicotinamide for the treatment of psoriasis. J Am Acad Dermatol 2010;63:775–81.

Li J, Bonkowski MS, Moniot S, Zhang D, Hubbard BP, Ling AJ, et al. A conserved NAD(+) binding pocket that regulates protein-protein interactions during aging. Science 2017;355(6331):1312–7.

Liu L, Su X, Quinn WJ 3rd, Hui S, Krukenberg K, Frederick DW, et al. Quantitative analysis of NAD synthesis-breakdown fluxes. Cell Metab 2018;27:1067–10680 e5.

Massudi H, Grant R, Braidy N, Guest J, Farnsworth B, Guillemin GJ. Age-associated changes in oxidative stress and NAD+ metabolism in human tissue. PLoS One 2012;7:e42357.

Matsumura H, Mohri Y, Binh NT, Morinaga H, Fukuda M, Ito M, et al. Hair follicle aging is driven by transepidermal elimination of stem cells via COL17A1 proteolysis. Science 2016;351(6273):aad4395.

Muiras ML, Muller M, Schachter F, Burkle A. Increased poly(ADP-ribose) polymerase activity in lymphoblastoid cell lines from centenarians. J Mol Med (Berl) 1998;76:346–54.

Navarrete-Solis J, Castanedo-Cazares JP, Torres-Alvarez B, Oros-Ovalle C, Fuentes-Ahumada C, Gonzalez FJ, et al. A double-blind, randomized clinical trial of niacinamide 4% versus hydroquinone 4% in the treatment of melasma. Dermatol Res Pract 2011;2011:379173.

Naylor RM, Baker DJ, van Deursen JM. Senescent cells: a novel therapeutic target for aging and age-related diseases. Clin Pharmacol Ther 2013;93:105–16.

Ok JS, Song SB, Hwang ES. Enhancement of replication and differentiation potential of human bone marrow stem cells by nicotinamide treatment. Int J Stem Cells 2018;11:13–25.

Panopoulos AD, Yanes O, Ruiz S, Kida YS, Diep D, Tautenhahn R, et al. The metabolome of induced pluripotent stem cells reveals metabolic changes occurring in somatic cell reprogramming. Cell Res 2012;22:168–77.

Quek LS, Grasset N, Jasmen JB, Robinson KS, Bellanger S. Dual role of the anaphase promoting complex/cyclosome in regulating stemness and differentiation in human primary keratinocytes. J Invest Dermatol 2018;138:1851–61.

Rheinwald JG, Green H. Serial cultivation of strains of human epidermal keratinocytes: the formation of keratinizing colonies from single cells. Cell 1975;6:331–43.

Shyh-Chang N, Daley GQ, Cantley LC. Stem cell metabolism in tissue development and aging. Development 2013;140:2535–47.

Siadat AH, Iraji F, Khodadadi M, Jary MK. Topical nicotinamide in combination with calcipotriol for the treatment of mild to moderate psoriasis: a double-blind, randomized, comparative study. Adv Biomed Res 2013;2:90.

Simon M, Green H. Enzymatic cross-linking of involucrin and other proteins by keratinocyte particulates in vitro. Cell 1985;40:677–83.

Son MJ, Son MY, Seol B, Kim MJ, Yoo CH, Han MK, et al. Nicotinamide overcomes pluripotency deficits and reprogramming barriers. Stem Cells 2013;31:1121–35.

Stein LR, Imai S. Specific ablation of Nampt in adult neural stem cells recapitulates their functional defects during aging. EMBO J 2014;33:1321–40.

Stratford MR, Rojas A, Hall DW, Dennis MF, Dische S, Joiner MC, et al. Pharmacokinetics of nicotinamide and its effect on blood pressure, pulse and body temperature in normal human volunteers. Radiother Oncol 1992;25:37–42.

Thierry F, Benotmane MA, Demeret C, Mori M, Teissier S, Desaintes C. A genomic approach reveals a novel mitotic pathway in papillomavirus carcinogenesis. Cancer Res 2004;64:895–903.

Wiley CD, Campisi J. From ancient pathways to aging cells-connecting metabolism and cellular senescence. Cell Metab 2016;23:1013–21.

Wiley CD, Velarde MC, Lecot P, Liu S, Sarnoski EA, Freund A, et al. Mitochondrial dysfunction induces senescence with a distinct secretory phenotype. Cell Metab 2016;23:303–14.

Yiasemides E, Sivapirabu G, Halliday GM, Park J, Damian DL. Oral nicotinamide protects against ultraviolet radiation-induced immunosuppression in humans. Carcinogenesis 2009;30:101–5.

Yoshino J, Mills KF, Yoon MJ, Imai S. Nicotinamide mononucleotide, a key NAD(+) intermediate, treats the pathophysiology of diet- and age-induced diabetes in mice. Cell Metab 2011;14:528–36.

Zhang H, Menzies KJ, Auwerx J. The role of mitochondria in stem cell fate and aging. Development 2018;145(8).

Zhang H, Ryu D, Wu Y, Gariani K, Wang X, Luan P, et al. NAD(+) repletion improves mitochondrial and stem cell function and enhances life span in mice. Science 2016;352(6292):1436–43.

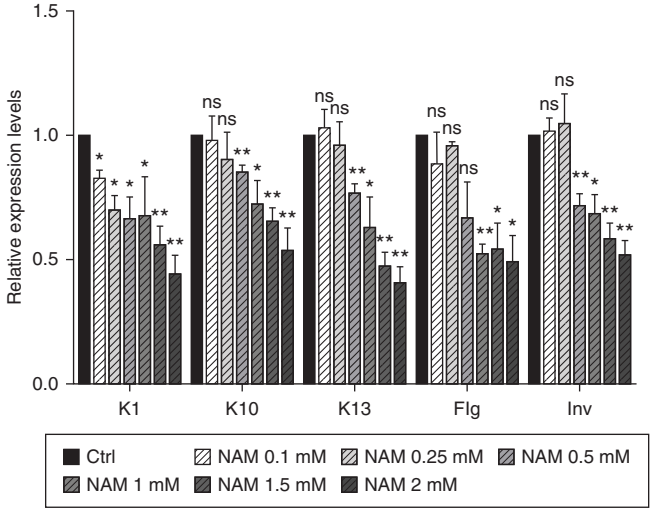

Supplementary Figure S1. NAM concentrations ranging from 0.5 mM to 2 mM prevent human primary keratinocyte differentiation. Reverse transcription quantitative PCR analyses performed after treatment of human primary keratinocytes (grown on 3T3-J2 feeders) with 0.1−2 mM NAM for 5 days. Statistical analyses: one sample *t* tests with a hypothetical value of 1. Data represent the means ± standard error of the mean, n = 5. Ctrl, untreated control cells; K1, keratin 1; K10, keratin 10; K13, keratin 13; Flg, filaggrin; Inv, involucrin; NAM, nicotinamide; ns, not significant.

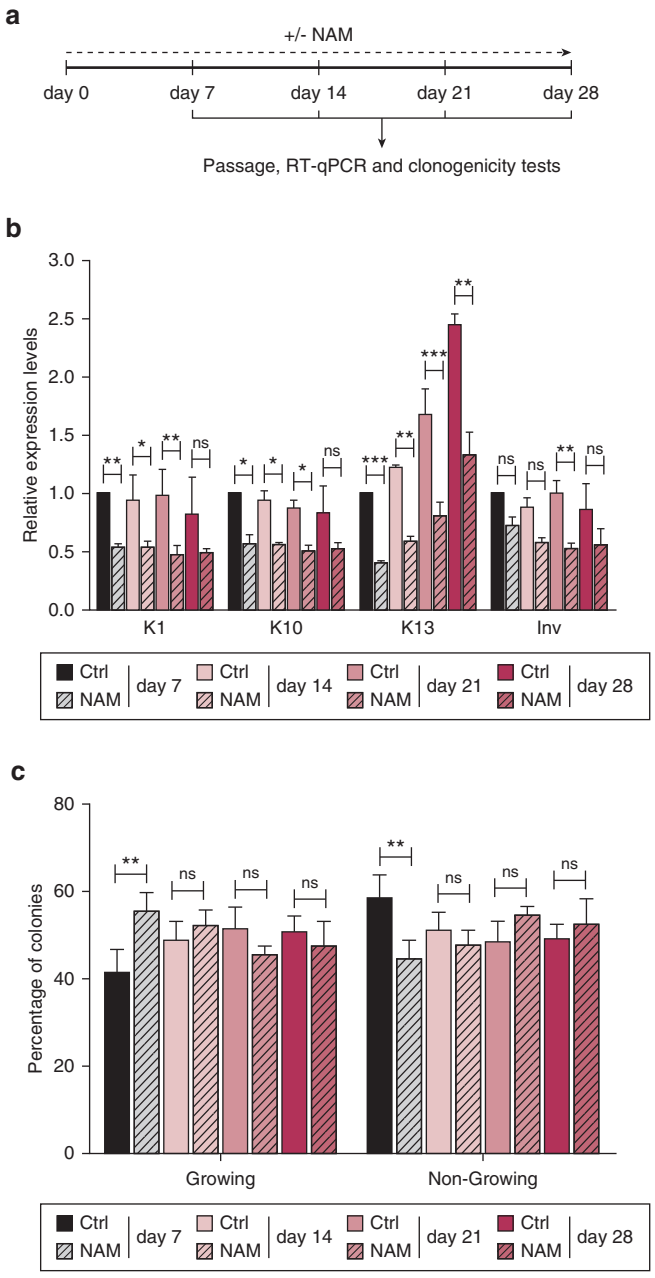

Supplementary Figure S2. Long-term effects of NAM on human primary keratinocyte differentiation and clonogenicity. (**a**) Experimental protocol: human primary keratinocytes were cultured on 3T3-J2 feeders and passaged every 7 days for 28 days ± NAM. At each passage, 400 cells were replated on a separate dish for clonogenicity tests and cultured for 12 days before Rhodamine B staining. (**b**) Reverse transcription quantitative PCR analyses of differentiation markers before each passage. Statistical analyses: two-way analysis of variance. Data represent the means ± standard error of the mean, n = 3. (**c**) Quantification of the growing (holoclones + meroclones) and non-growing (paraclones) colonies before each passage. Statistical analyses: two-way analysis of variance. Data represent the means ± standard error of the mean, n = 3. Ctrl, untreated control cells; Inv, involucrin; K1, keratin 1; K10, keratin 10; K13, keratin 13; NAM, nicotinamide; ns, not significant.

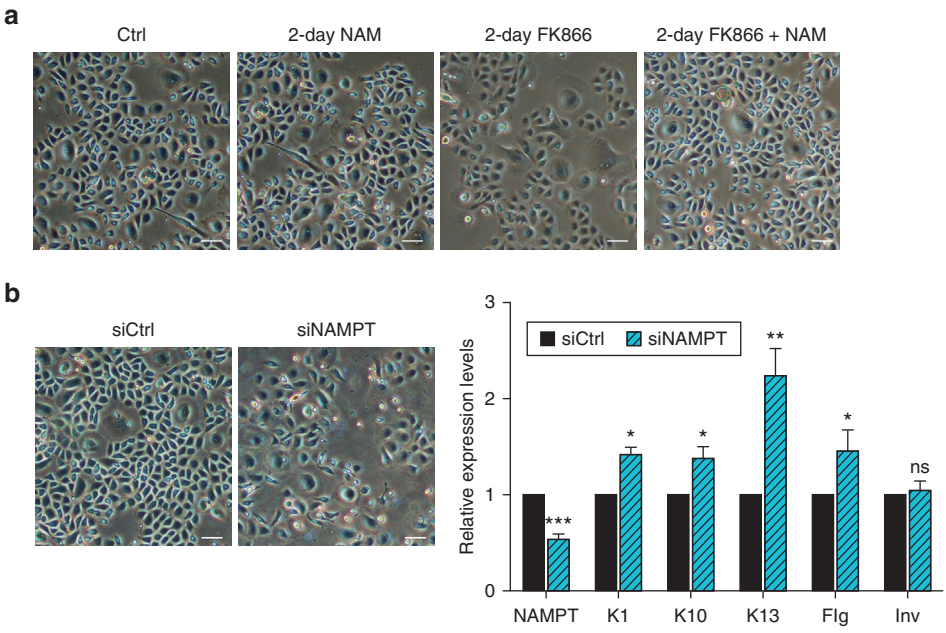

Supplementary Figure S3. NAMPT inhibition induces human primary keratinocyte differentiation. (**a**) Phase-contrast images of human primary keratinocytes treated with NAM, FK866, or both, as indicated. Pictures were taken on the inverted Nikon Eclipse TS100. Scale bar = 75 μm. (**b**) Transfections were performed in Dermalife medium (LL-0007; Lifeline Cell Technology, Oceanside, CA) with predesigned ON-TARGETplus SMARTpool siRNA targeting NAMPT (L-004581-00-0020; Dharmacon, Lafayette, CO) or non-targeting control small interfering RNA (D-001810-01-50; Dharmacon) at the final concentration of 100 nM using DharmaFECT 1 (Dharmacon), according to the manufacturer's instructions. Cells were photographed 3 days after small interfering RNA treatment and harvested for reverse transcription quantitative PCR analyses. Left panel: Phase contrast images of cells treated with either Ctrl or NAMPT small interfering RNAs. Pictures were taken on the inverted Nikon Eclipse TS100. Scale bar = 75 μm. Right panel: reverse transcription quantitative PCR analyses of differentiation markers after small interfering RNA–mediated silencing. Statistical analyses: one sample *t* tests with a hypothetical value of 1. Data represent the means ± standard error of the mean, n = 6. Ctrl, untreated control cells; Flg, filaggrin; Inv, involucrin; K1, keratin 1; K10, keratin 10; K13, keratin 13; NAM, nicotinamide; ns, not significant.

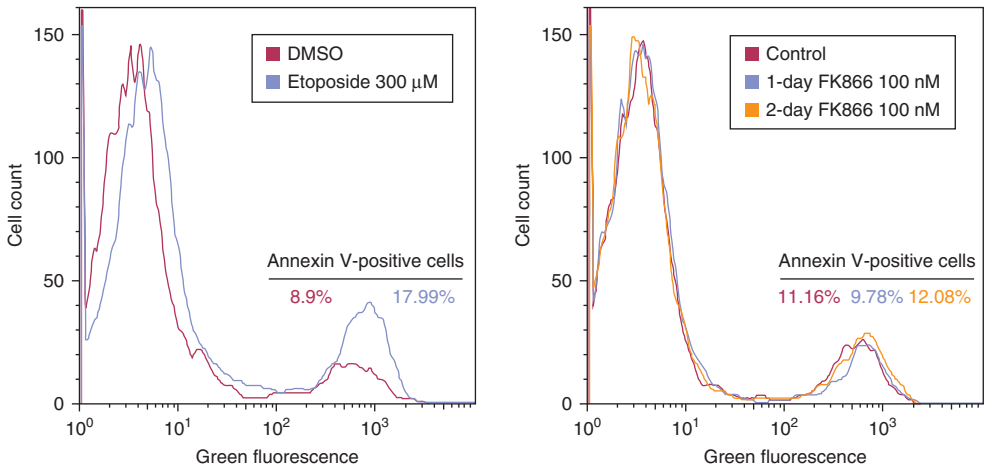

Supplementary Figure S4. FK866 treatment does not induce apoptosis. Left panel: Flow cytometry analyses showing the Annexin signal (559935, Annexin V; BD Biosciences, San Jose, CA) in cells treated with DMSO or etoposide (used as a positive control). Right panel: Flow cytometry analyses showing the Annexin signal in cells treated as indicated.

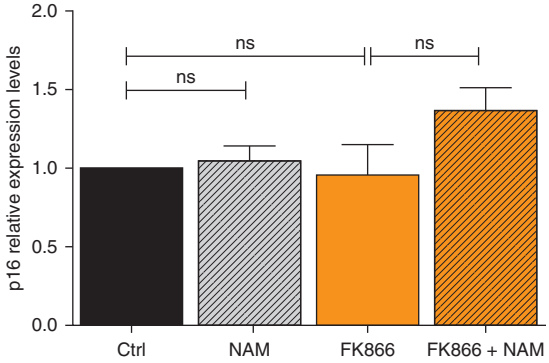

Supplementary Figure S5. p16 is not modulated by FK866 treatment. Reverse transcription quantitative PCR analyses of p16 after treatment as indicated. Statistical analyses: paired *t* tests. Data represent the means ± standard error of the mean, n = 4. Ctrl, untreated control cells; NAM, nicotinamide.

Supplementary Table S1. Primer sequences for reverse transcription quantitative PCR

Primer name	Sequence (5′-3′)
TBP	F: CGTCCCAGCAGGCAACAC R: TTGTGAGAGTCTGTGAGTGGAAGAG
Keratin 1	F: CTTCTTCAGCCCCTCAATGTG R: GCTCCCTTTCTCGAGACTTCAC
Keratin 10	F: GCTGGCAGCTGATGACTTCAG R: TACGCAGGCCGTTGATGTC
Keratin 13	F: CTTTGTTGACTTTGGTGCTTGTG R: GTTGAGGTTCTGCATGGTGATC
Involucrin	F: CCATCAGGAGCAAATGAAACAG R: GCTCGACAGGCACCTTCTG
Filaggrin	F: GTGTTAGTTACAATTCCAATCCTGTTG R: ATACGTTGCATAATACCTTGGATGATC
NAMPT	F: GCAGAAGCCGAGTTCAACATC R: TGCTTGTGTTGGGTGGATATTG
Lamin B1	F: CGCTTGGTAGAGGTGGATTCTG R: CCTCACTTGGGCATCATGTTG
p21	F: GCGACTGTGATGCGCTAATG R: CGGTGACAAAGTCGAAGTTCC
p16	F: CCCAACGCACCGAATAGTTAC R: CGCTGCCCATCATCATGAC

F, forward; R, reverse; TBP, TATA-binding protein.

Supplementary Table S2. Primary antibodies used for immunofluorescence, Western blotting, and immunohistochemistry

Primary antibody	Dilution	Source (catalogue number; supplier)
Immunofluorescence		
Ki-67	1:500	ab15580; Abcam, Cambridge, UK
K13	1:200	Novocastra NCL-CK13; Leica Biosystems, IL
Western blotting		
K1/K10	1:100	CBL266; Merck Millipore, Darmstadt, Germany
K13	1:500	Novocastra NCL-CK13; Leica Biosystems, IL
Involucrin	1:500	Novocastra NCL-INV; Leica Biosystems, IL
Ki-67	1:1000	ab15580; Abcam, Cambridge, UK
Actin	1:1000	A2066; Sigma-Aldrich, MO
β-tubulin	1:5000	T4026; Sigma-Aldrich, MO
Immunohistochemistry		
K10	1:100	DE-K10, M7002, DAKO, Agilent, CA
Filaggrin	1:200	FLG/1561, ab218395; Abcam, Cambridge, UK
Loricrin	1:500	EPR7148(2)(B), ab176322; Abcam, Cambridge, UK
Ki-67	1:500	MIB-1; M7240; DAKO, Agilent, CA